Supporting Information for

An unusual three-dimensional Dy-Cd_2 Framework exhibiting single-ion magnet behavior

Xue-Jing Zhang, Ke Liu, Yan-Min Bing, Na Xu*, Wei Shi and Peng Cheng*

Materials and General Characterization. All chemicals applied were of reagent grade and used as received without further refinement. Elemental analyses for C, H and N were performed on a Perkin-Elmer elemental analyzer. Powder X-ray diffraction (PXRD) measurements were recorded on a D/Max-2500 X-ray diffractometer using Cu-Kα radiation. Thermogravimetric analyses were performed on a Labsys NETZSCH TG 209 Setaram apparatus with heating rate of 10 °C/min in Nitrogen atmosphere. Magnetic data were collected on a Quantum Design SQUID MPMS XL-7 magnetometer. Diamagnetic corrections were made with Pascal's constants for all the sample holders and constituent atoms.

Synthesis of $[TbCd_2(PIDC)(HPIDC)(H_2O)_5Cl_2]\cdot 3H_2O$ (**1**): A mixture of H_3PyIDC (0.0126 g, 0.05 mmol), $TbCl_3\cdot 6H_2O$ (0.0371 g, 0.1 mmol), $CdCl_2$ (0.0456 g, 0.2 mmol), LiOH (0.0042 g, 0.1 mmol), 4 mL H_2O and 1 mL CH_3OH were sealed into a 25 mL Teflon-lined Parr and heated to 120°C for 72 h under autogenously pressure. After cooling to room temperature at a rate of 2 °C/h, long strip flavescens crystals suitable for X-ray diffraction analysis were collected, washed with water, and dried in air. Yield: 65% based on Tb. Elemental analysis found (Calcd.) for $C_{20}H_{25}Cd_2Cl_2TbN_6O_{16}$: C 22.78 (22.66), H 1.81 (2.37), N 7.97 (7.93).

$[DyCd_2(PIDC)(HPIDC)(H_2O)_5Cl_2]\cdot 3H_2O$ (**2**) were synthesized by a similar method as **1** using $DyCl_3\cdot 6H_2O$ instead of $TbCl_3\cdot 6H_2O$. Yield: 68% based on Dy. Elemental analysis found (Calcd.) for $C_{20}H_{25}Cd_2Cl_2DyN_6O_{16}$: C 22.71(22.58), H 1.81(2.37), N 7.94 (7.90).

The magnetic-site dilution sample **$\{[Dy_{0.035}Y_{0.965}Cd_2(PIDC)(HPIDC)(H_2O)_5Cl_2]\cdot 3H_2O\}_n$** (**3**) was obtained by adding $DyCl_3\cdot 6H_2O$ and $YCl_3\cdot 6H_2O$ (molar ratio of 1:30) together in the same synthesis condition of **2**. The phase purity was checked by PXRD (Fig. S1). The molar ratio of Dy:

Y was 1:27.57 by ICP analysis. Elemental analysis found (Calcd.) for $C_{20}H_{25}Cd_2Cl_2Dy_{0.035}Y_{0.965}N_6O_{16}$: C 24.27 (24.20), H 2.53 (2.54), N 8.28 (8.47).

Crystallographic Studies

Crystallographic data of **1** and **2** were collected on an Oxford Supernova Single Crystal Diffractometer, which was equipped with graphite monochromatic Mo-Kα radiation (λ = 0.71073 Å). Structures were solved by direct methods and refined by full-matrix least-squares techniques on F^2 with the *SHELXS-97* and *SHELXL-97* program package.[1] Anisotropic thermal parameters were assigned to all non-hydrogen atoms. The formulas were identified by combining single-crystal structure, element analysis and thermogravimetric analysis. The crystallographic data for **1** and **2** are listed in Table S3. CCDC 1033271 and 1033270 for **1** and **2** contains the supplementary crystallographic data for this paper. The data can be obtained free of charge from the Cambridge Data Centre (www.ccdc.cam.ac.uk/data_request/cif).

Ref S1. M. Sheldrick, *Acta Cryst.*, 2008, **A64**, 112 – 122.

Table S1 SHAPE Analysis of Dy^{III} cation in **2**.[a]

Label	SHAPE	Symmetry	Distortion
OP-8	Octagon	D_{8h}	29.557
HPY-8	Heptagonal pyramid	C_{7v}	23.435
HBPY-8	Hexagonal bipyramid	D_{6h}	15.236
CU-8	Cube	O_h	8.463
SAPR-8	Square antiprism	D_{4d}	0.526
TDD-8	Triangular dodecahedron	D_{2d}	1.737
JGBF-8	Johnson gyrobifastigium J26	D_{2d}	15.308
JETBPY-8	Johnson elongated triangular bipyramid J14	D_{3h}	26.742
JBTPR-8	Biaugmented trigonal prism J50	C_{2v}	2.804
BTPR-8	Biaugmented trigonal prism	C_{2v}	2.330
JSD-8	Snub diphenoid J84	D_{2d}	4.657
TT-8	Triakis tetrahedron	T_d	9.288
ETBPY-8	Elongated trigonal bipyramid	D_{3h}	21.685

[a] (a) SHAPE, version 2.0; Continuous Shape Measures Calculation; Electronic Structure Group, Universiat de Barcelona: Barcelona, Spain, 2010. (b) D. Casanova, M. Liunell, P. Alemany, S. Alvarez, *Chem. Eur. J.*, 2005, **11**, 1479 – 1494. D_{4d} symmetry was suggested by the calculation with the minimum distortion value.

Table S2 Structural Parameters of the Lanthanide Coordination Sphere in **2**.

Φ	45.4	45.6	38.9	53.2	35.7	54.4	39.5	47.4
α	60.4	53.1	58.4	59.5	57.3	53.1	58.1	58.1
d_{in}	2.855(9)	2.737(9)	2.694(9)	2.875(9)	2.813(9)	2.703(9)	2.828(9)	2.863(9)
d_{pp}	2.538(2)							

Table S3 Crystal data and structural refinements for **1** and **2**.

	1	**2**
formula	$C_{20}H_{25}Cd_2Cl_2TbN_6O_{16}$	$C_{20}H_{25}Cd_2Cl_2DyN_6O_{16}$
M / g mol^{-1}	1060.08	1063.66
cryst syst	monoclinic	monoclinic
space group	*Cc*	*Cc*
a / Å	12.5247(5)	12.5087(11)
b / Å	32.2184(16)	32.165(2)
c / Å	7.6101(5)	7.6022(5)
α / deg	90	90
β / deg	98.856(4)	98.833(7)
γ / deg	90	90
V / Å^3	3034.3(3)	3022.4(4)
Z	4	4
reflns collected	5955	5854
unique reflns	3624	4031
R_1[a] [$I > 2\sigma(I)$]	0.0321	0.0235
wR_2[b] (all data)	0.0683	0.0622
GOF on F^2	1.027	1.108

Table S4 Selected bond lengths (Å) and bond angles (deg) for **2**

Dy(1)-O(10)#1	2.370(5)	O(4)-Dy(1)-O(1)	137.3(2)
Dy(1)-O(6)	2.350(5)	O(4)-Dy(1)-O(7)	112.9(2)
Dy(1)-O(7)	2.370(6)	O(4)-Dy(1)-O(2)	72.5(2)
Dy(1)-O(2)	2.348(6)	O(4)-Dy(1)-O(3)	76.8(2)
Dy(1)-O(3)	2.371(5)	O(4)-Dy(1)-O(11)#1	78.18(16)
Dy(1)-O(4)	2.273(5)	O(4)-Dy(1)-O(1)	137.3(2)
Dy(1)-O(11)#1	2.368(6)	O(11)#1-Dy(1)-O(10)#1	74.03(19)
Dy(1)-O(1)	2.349(6)	O(11)#1-Dy(1)-O(3)	72.8(2)
Cd(1)-O(12)	2.216(5)	O(1)-Dy(1)-O(6)	78.0(2)
Cd(1)-N(2)#4	2.240(6)	O(1)-Dy(1)-O(7)	87.99(18)
Cd(1)-O(5) #4	2.364(5)	O(1)-Dy(1)-O(3)	145.9(2)
Cd(1)-O(13)	2.373(6)	O(1)-Dy(1)-O(11)#1	110.5(2)
Cd(1)-Cl(1)	2.446(2)	N(1)-Cd(2)-O(8)	71.0(2)
Cd(2)-N(1)	2.313(6)	N(1)-Cd(2)-N(6)	80.6(2)
Cd(2)-O(8)	2.358(5)	N(1)-Cd(2)-Cl(2)#3	149.79(16)
Cd(2)-O(9)	2.355(6)	N(1)-Cd(2)-O(9)	108.6(2)
Cd(2)-N(6)	2.363(6)	O(8)-Cd(2)-N(6)	108.9(2)
Cd(2)-Cl(2)	2.5347(19)	O(8)-Cd(2)-Cl(2)	96.90(14)
Cd(2)-Cl(2)#3	2.6120(19)	O(8)-Cd(2)-O(9)	178.20(19)
O(6)-Dy(1)-O(10)#1	136.35(17)	N(6)-Cd(2)-Cl(2)	153.97(16)

O(6)-Dy(1)-O(7)	70.0(2)	N(6)-Cd(2)-Cl(2A)	86.90(16)
O(6)-Dy(1)-O(3)	118.31(19)	Cl(2)-Cd(2)- Cl(2A)	98.05(2)
O(6)-Dy(1)-O(11)#1	147.5(2)	N(2)#4-Cd(1)-Cl(1)	106.15(18)
O(7)-Dy(1)-O(10)#1	78.8(2)	N(2)#4-Cd(1)-O(13)	105.5(2)
O(7)-Dy(1)-O(3)	72.2(2)	N(2)-Cd(1)-O(5)#4	73.5(2)
O(7)-Dy(1)-O(11)#1	139.3(2)	O(13)-Cd(1)-Cl(1)	101.41(16)
O(2)-Dy(1)-O(10)#1	116.51(19)	O(5)#4-Cd(1)-Cl(1)	100.20(14)
O(2)-Dy(1)-O(6)	78.56(19)	O(5)#4-Cd(1)-O(13)	157.75(19)
O(2)-Dy(1)-O(7)	144.8(2)	O(12)-Cd(1)-N(2)#4	128.9(2)
O(2)-Dy(1)-O(3)	139.52(18)	O(12)-Cd(1)-Cl(1)	119.41(16)
O(2)-Dy(1)-O(11)#1	75.6(2)	O(12)-Cd(1)-O(13)	88.1(2)
O(2)-Dy(1)-O(1)	69.8(2)	O(12)-Cd(1)-O(5)#4	76.7(2)
O(3)-Dy(1)-O(10)#1	78.0(2)		
O(4)-Dy(1)-O(10)#1	146.8(2)		
O(4)-Dy(1)-O(6)	75.5(2)		

Symmetry operation code: $^{\#1}$1+X, +Y, +Z; $^{\#3}$+X, 1-Y, 1/2+Z; $^{\#4}$-1/2+X, 3/2-Y, 1/2+Z.

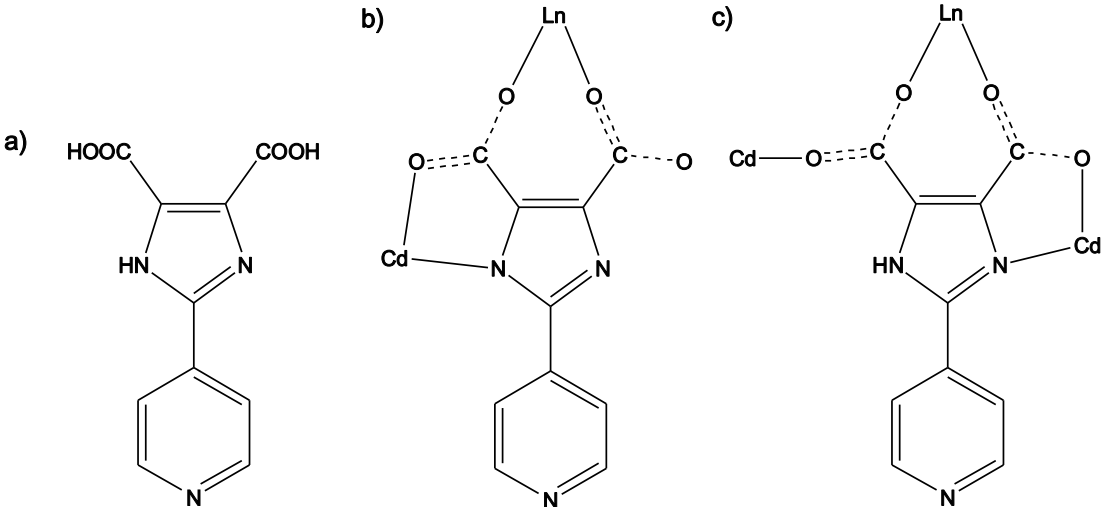

Scheme S1 The structural formula of H_3PIDC (a) and the coordination modes of $PIDC^{3-}$ (b) and $HPIDC^{2-}$ (c) in **1** and **2**.

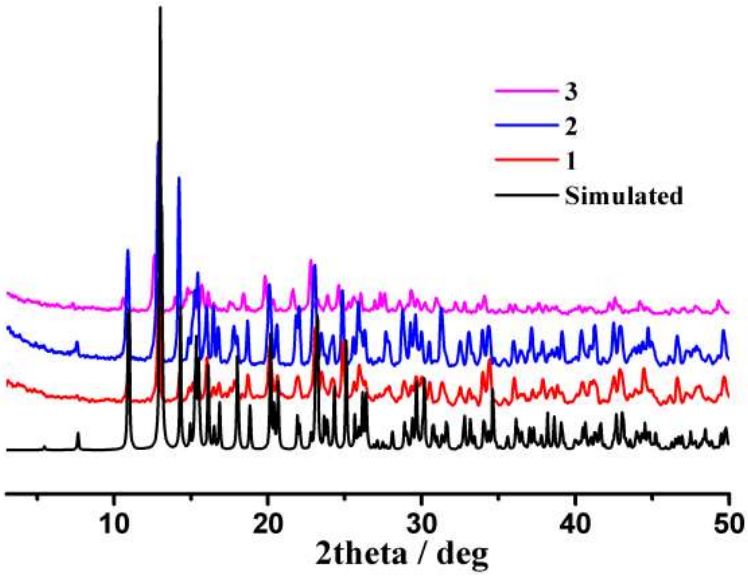

Fig. S1 Simulated and measured PXRD of **1**-**3**.

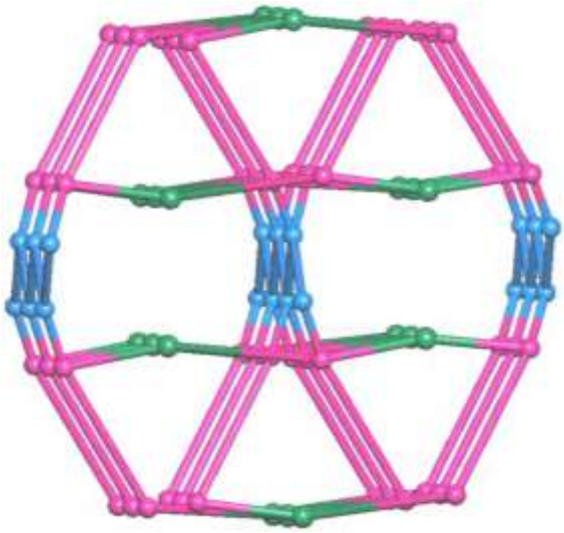

Fig. S2 View of the 3, 4, 4-connected topological structure.

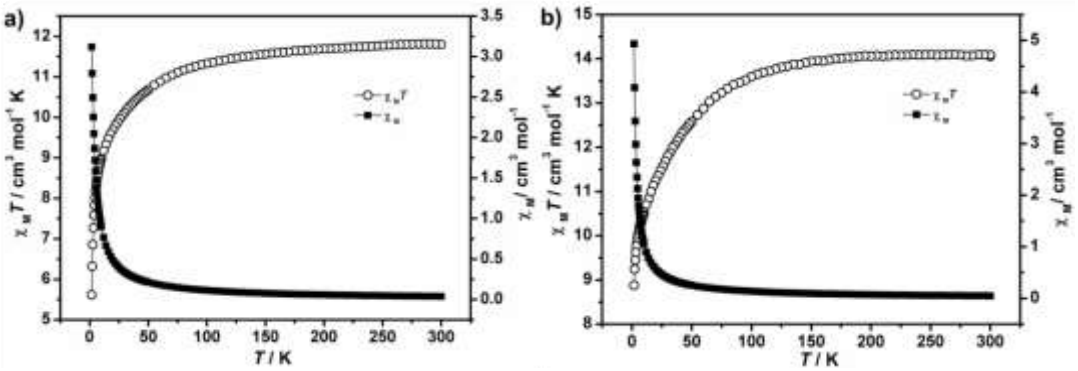

Fig. S3 Temperature dependence of χ_M (■) and $\chi_M T$ (O) of **1** (a) and **2** (b).

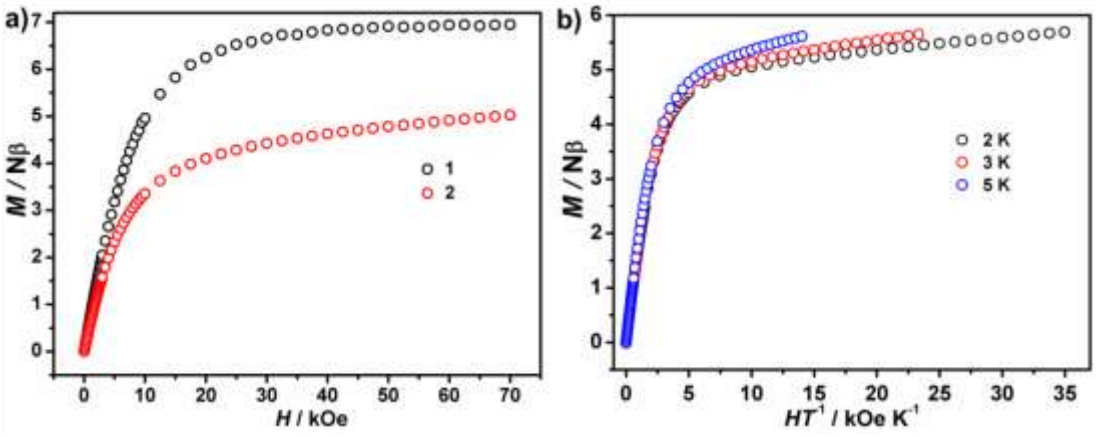

Fig. S4 Field dependence of the magnetizations of **1** and **2** (a) and plot of M vs. HT^{-1} at 2, 3 and 5 K for **2** (b).

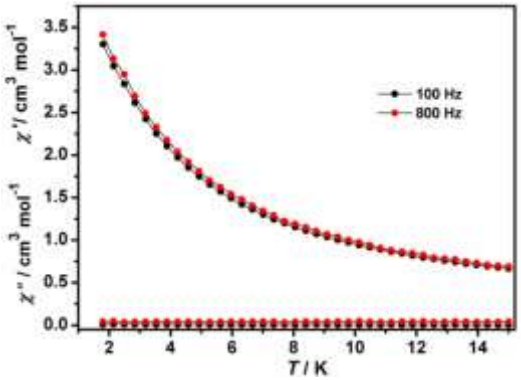

Fig. S5 Temperature dependence of the ac susceptibilities of **1** at zero dc field.

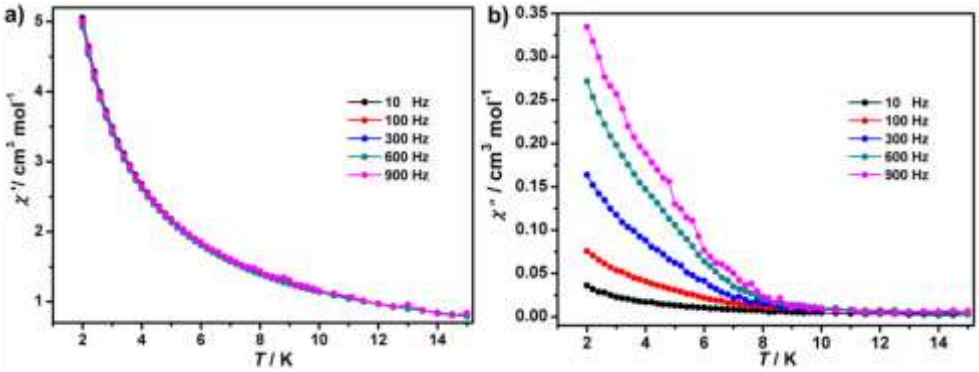

Fig. S6 Temperature dependence of the in-phase (χ') and out-of-phase (χ'') ac susceptibilities of **2** at zero dc field.

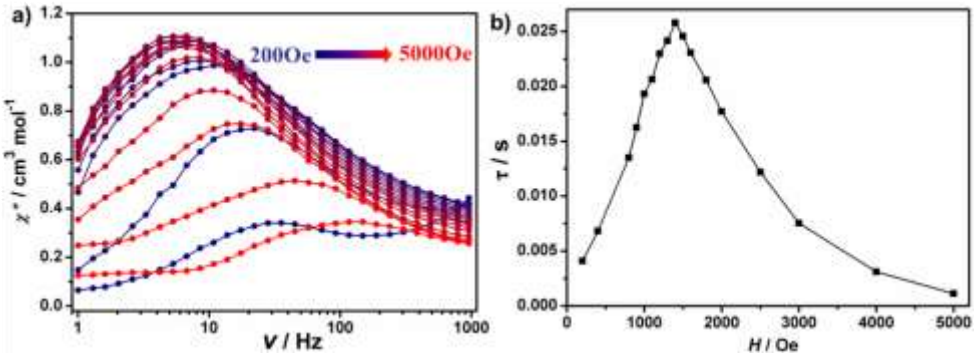

Fig. S7 a) Frequency dependence of the out-of-phase (χ'') ac susceptibility components for **2** measured at 2 K with different dc fields. b) Field dependence of the relaxation time from χ'' vs. υ data.

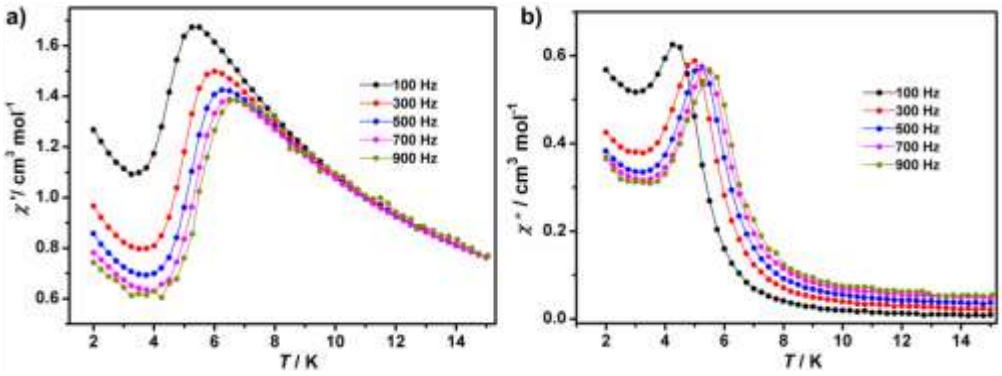

Fig. S8 Temperature dependence of the in-phase (χ') and out-phase (χ'') ac susceptibilities of **2** at the indicated field of 1400 Oe.

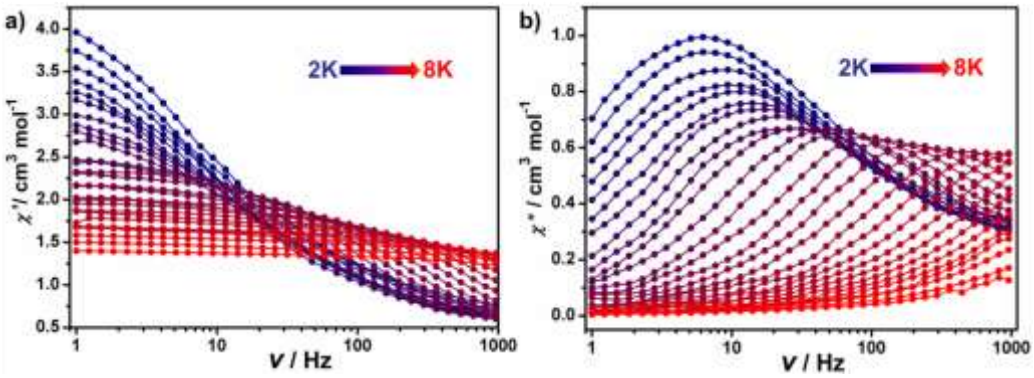

Fig. S9 Frequency dependence of the in-phase (χ') and out-phase (χ'') ac susceptibilities of **2** at the indicated field of 1400 Oe.

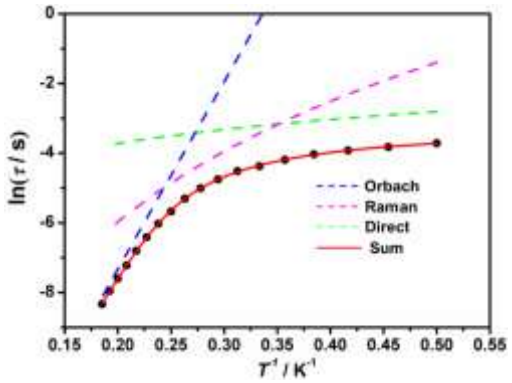

Fig. S10 Plot of ln(τ) versus 1/T for **2**, obtained under an applied field of 1400 Oe. The red line represents the fit to the experimental data using Eq. 1 (main text). Blue, green and pink dashed lines represent individual Orbach, direct and Raman fits, respectively.

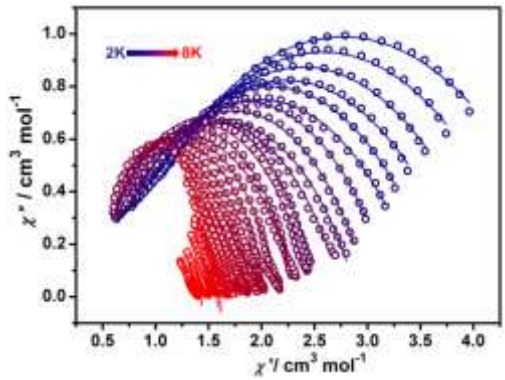

Fig. S11 Cole-Cole diagram for **2** extracted by plotting χ'' vs. χ' and fitted by a generalized Debye model.

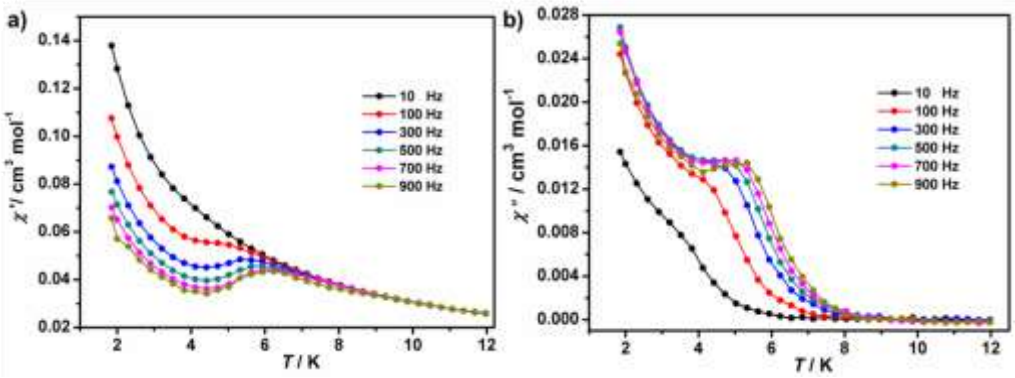

Fig. S12 Temperature dependence of the in-phase (χ') and out-phase (χ'') AC susceptibilities of **3** at zero dc field.

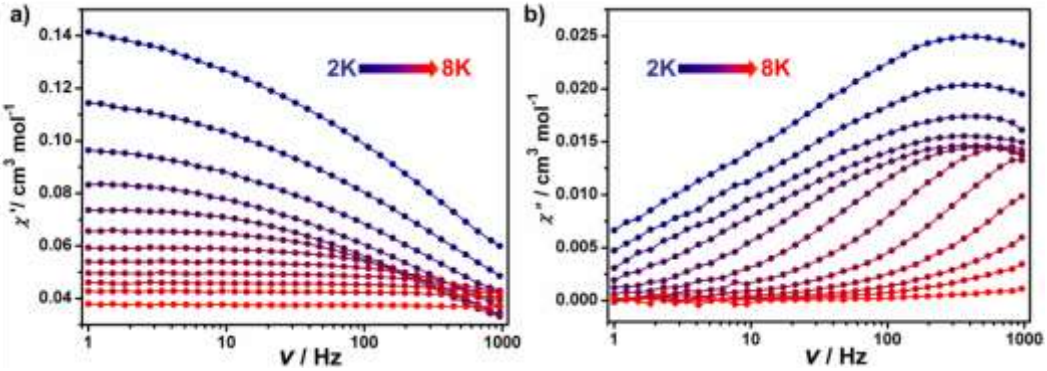

Fig. S13 Frequency dependence of the in-phase (χ') and out-phase (χ'') ac susceptibilities of **3** at zero dc field.

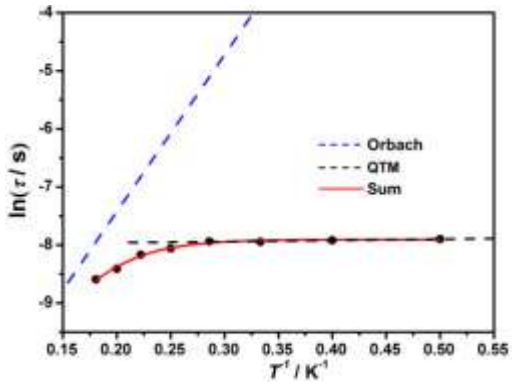

Fig. S14 Plot of ln(τ) versus 1/T for **3**, obtained under an dc field of 0 Oe. The red line represents the fit to the experimental data using Eq. 1 (main text). Blue and black dashed lines represent individual Orbach and QTM fits, respectively.

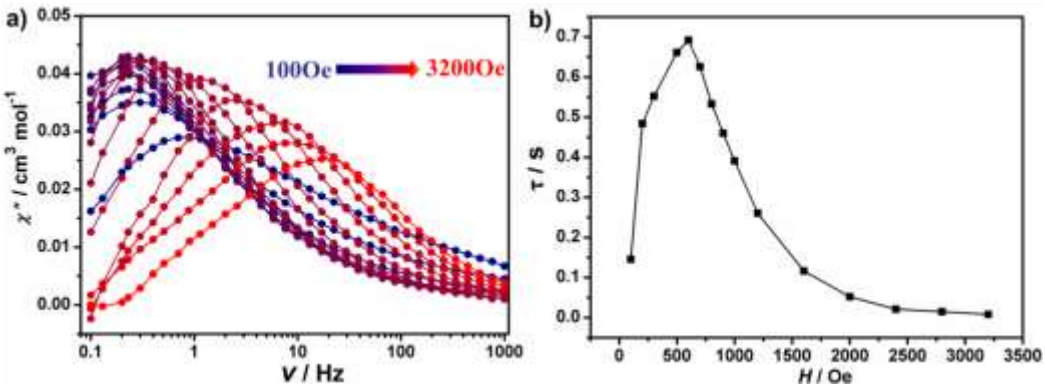

Fig. S15 a) Frequency dependence of the out-of-phase (χ'') ac susceptibility components for **3** measured at 2 K with different dc fields. b) Field dependence of the relaxation time.

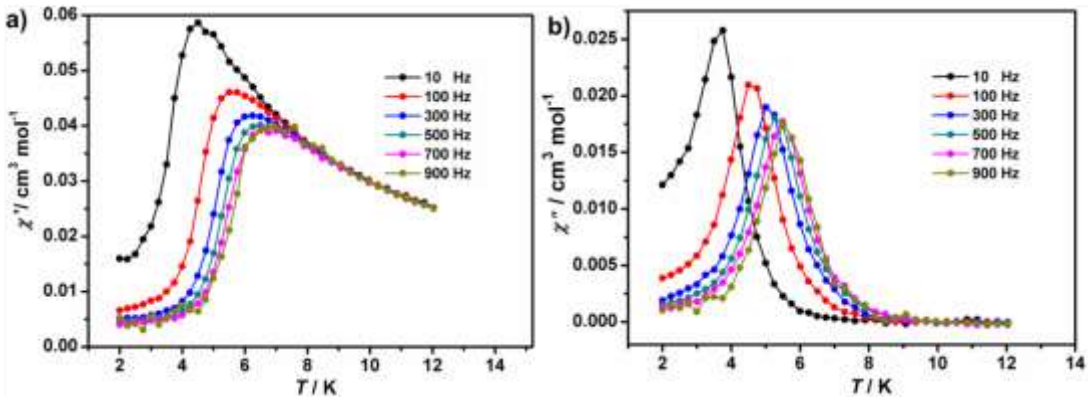

Fig. S16 Temperature dependence of the in-phase (χ') and out-phase (χ'') AC susceptibilities of **3** at the indicated field of 600 Oe.

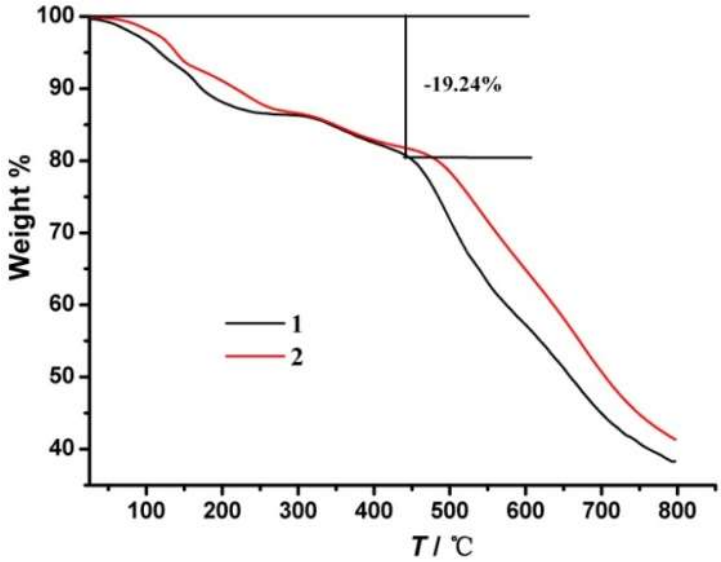

Fig. S17 TGA of **1** and **2**.

Table S5 The parameters of the Cole-Cole plots fitted by the general Debye models.

2 (1400 Oe dc field)

T / K	χ_0	χ_1	α	T / K	χ_0	χ_1	α	T / K	χ_0	χ_1	α
2.0	0.535	5.001	0.460	3.8	0.335	2.790	0.377	5.6	0.268	2.052	0.249
2.2	0.547	4.616	0.454	4.0	0.384	2.531	0.280	5.8	0.076	2.005	0.305
2.4	0.535	4.244	0.440	4.2	0.403	2.448	0.271	6.0	0.080	1.925	0.301
2.6	0.437	3.998	0.449	4.4	0.397	2.306	0.243	6.2	0	1.869	0.302
2.8	0.468	3.713	0.419	4.6	0.293	2.304	0.300	6.4	0	1.795	0.285
3.0	0.427	3.544	0.431	4.8	0.322	2.143	0.247	6.6	0	1.739	0.287
3.2	0.401	3.267	0.394	5.0	0.268	2.052	0.243	6.8	0	1.701	0.313
3.4	0.442	3.034	0.365	5.2	0.076	2.005	0.300	7.0	0	1.646	0.303
3.6	0.401	2.908	0.380	5.4	0.080	1.925	0.247	7.5	0	1.420	0.145

3 (600 Oe dc field)

T / K	χ_0	χ_1	α	T / K	χ_0	χ_1	α	T / K	χ_0	χ_1	α
2.0	0.005	0.161	0.402	3.8	0.005	0.077	0.198	5.6	0.010	0.052	0.137
2.2	0.004	0.147	0.406	4.0	0.005	0.074	0.227	5.8	0.011	0.050	0.137
2.4	0.004	0.137	0.404	4.2	0.005	0.070	0.219	6.0	0.016	0.047	0.117
2.6	0.005	0.125	0.385	4.4	0.005	0.067	0.215	6.2	0.022	0.047	0.115
2.8	0.004	0.117	0.378	4.6	0.004	0.064	0.225	6.4	0.023	0.046	0.136
3.0	0.004	0.106	0.347	4.8	0.005	0.059	0.144	6.6	0.025	0.044	0.323

3.2	0.004	0.097	0.310	5.0	0.006	0.058	0.139	6.8	0.027	0.043	0.160
3.4	0.005	0.089	0.272	5.2	0.007	0.055	0.129	7.0	0.017	0.043	0.259
3.6	0.004	0.084	0.263	5.4	0.009	0.054	0.139	7.5	0.03	0.04	0.182